Noname manuscript No.
(will be inserted by the editor)

Fully Automated 2D and 3D Convolutional Neural Networks Pipeline for Video Segmentation and Myocardial Infarction Detection in Echocardiography

Oumaima Hamila · Sheela Ramanna · Christopher J. Henry · Serkan Kiranyaz · Ridha Hamila · Rashid Mazhar · Tahir Hamid

Received: date / Accepted: date

Abstract Cardiovascular imaging machines for disease diagnosis are widely used to produce multiple types of data such as images and videos, which cardiologists use to diagnose their patients of the right cardiac deficiency. However, these machines deliver an abundant amount of data that demands quick analysis in order to assign the adequate treatment. Furthermore, the acquired data quality varies depending on the acquisition conditions and the patient's responsiveness to the setup instructions. These constraints are challenging to doctors especially when patients are facing myocardial infarction (MI) and their lives are at stake. In this paper, we propose an innovative real-time end-to-end fully automated model based on convolutional neural networks (CNN) to detect MI from videos produced by echocardiography, which is a non-invasive cardiovascular imaging tool that plays a major role in the diagnosis of patients affected or suspected with MI. Our model is implemented as a pipeline consisting of a 2D CNN that performs data preprocessing by segmenting the left ventricle (LV) chamber from the apical four-chamber (A4C) view, followed by a 3D CNN that performs a binary classification to detect if the segmented echocardiography shows signs of MI. We trained both CNNs on a dataset composed of 165 echocardiography videos each acquired from a distinct patient. The 2D CNN achieved an accuracy of 97.18% on data segmentation while the 3D CNN achieved 90.9% of accuracy, 100% of precision and 95% of recall on MI detec-

Oumaima Hamila, Sheela Ramanna, Christopher J. Henry
Department of Applied Computer Science, The University of Winnipeg
515 Portage Avenue, Winnipeg, MB Canada, R3B 2E9
E-mail: hamila-o@webmail.uwinnipeg.ca, {s.ramanna,ch.henry}@uwinnipeg.ca

Serkan Kiranyaz, Ridha Hamila
Department of Electrical Engineering, Qatar University, Doha, Qatar
E-mail: {mkiranyaz,hamila}@qu.edu.qa

Tahir Hamid, Rashid Mazhar
Department of Cardiology, Hamad Medical Corporation, Doha, Qatar
E-mail: tahirhamid76@yahoo.co.uk, rashmazhar@hotmail.com

tion. Our results demonstrate that creating a fully automated system for MI detection is feasible and propitious.

Keywords 3D Convolutional Neural Network · Video Segmentation · Myocardial Infarction · Detection · Echocardiography

1 Introduction

According to the World Health Organization, cardiovascular diseases (CVD) are responsible for 30% of the annual mortality rate, affecting roughly 18 million humans worldwide [1]-[2]. One of the prevalent cardiovascular disorders is acute myocardial infarction (AMI) [3], commonly referred to as heart attack, and it is pathologically defined as the death of the myocardial cells due to an extended ischemia (limitation of the blood supply to the tissues) [4]. As soon as ischemia happens, in most cases, the patient starts showing various clinical symptoms such as chest pain or epigastric discomfort [5] which, if not treated in critical time, will eventually lead to the death of the myocardial cells and to an infarction [6].

Considering the alarming statistics revealed about myocardial infarction (MI) death rates, specialists proclaim the urgent need to integrate machine learning (ML) and deep learning (DL) into health-care systems to provide advanced and personalized assistance to patients [7]-[8]. Cardiovascular imaging techniques, in particular, witnessed an evolution during the last two decades [9] which enabled cardiologists to further develop their understanding of the pathologies. Nevertheless, studies [10]-[11] show that relying on classical approaches to understanding the data generated by cardiovascular imaging machines is insufficient and requires modernization by integrating ML into the process of data acquisition and processing. The tremendous ability of ML and its powerful capability of analyzing a large quantity of data in a short time while producing results of high accuracy and precision [12]-[13], would ameliorate the diagnosis of CVD and eventually elevate the chances of patients in receiving a more targeted and customized treatment [14].

Echocardiography as a cardiac imaging test used in particular by cardiologists, is highly recommended by The American Society of Echocardiography in view of its capability to assess both the cardiac function and structure [15]. The test generates rapid, non-invasive and real-time views of the cardiac chambers, offering detailed visualization of the heart's functional and structural state from different angles and planes, which allow cardiologists to predict signs of MI in a patient almost instantaneously [16]. These features are unavailable in other bedside assessments, hence echocardiography is becoming indispensable to cardiologists [17]. Nonetheless, echocardiography tests produce large and complex data that needs to be entirely exploited and understood in order to make a complete diagnosis based on visual interpretation [7], which is highly dependent on the level of experience of the cardiologist in question [18]. Moreover, in some cases, an important amount of the generated data remain unused due to insufficient time and difficulty in interpretation [19]. Furthermore, data acquisition is usually performed in emergencies, which often yields images of low quality [20]-[21]. Consequently, this significantly decreases the accuracy of the diagnosis [22]. Therefore, cardiologists along with researchers, have been investigating the possibility of integrating automatic programs into cardiovascular imaging machines to create a more reliable diagnosis process [23]-[24].

To address some of the above issues, several approaches have been developed in order to estimate the cardiac motion or mass. Some of which are based on signal-processing analysis such as Fourier tracking [25], or metaheuristics such as genetic algorithms [26], while some others use ML and convolutional neural networks (CNN) [27]-[28]. However, these methods either heavily rely on very specific and limited conditions of data acquisition (high-resolution echocardiograms, high frame-rate, minimal noise) [24], or require the technician or the cardiologist to perform preliminary preprocessing steps to be able to proceed with the prediction process [29].

In this paper, we propose a method to overcome the following issues: i) subjective reading of the data that relies on expert cardiologists, ii) generated poor-quality videos, iii) massive amounts of video preprocessing, and iv) manual visual MI detection. Thus, the proposed solution is a of fully automated pipeline consisting of a 2D CNN that performs data preprocessing followed by a 3D CNN that performs binary classification to detect MI from echocardiography videos. As a matter of fact, the occurrence of MI is strongly dependent on signs of abnormalities shown in the behavior of the left ventricle (LV) wall motion or volume [30], which is the bottom left chamber of the heart. Therefore, our proposed pipeline begins with a 2D CNN that segments the LV from an echocardiography video. Then, the segmented video is fed to a 3D CNN, which extracts the relevant spatio-temporal features from it and uses these features to detect the presence of MI. The input to the pipeline is an unprocessed echocardiography acquired by a technician or a cardiologist from a patient, and the output is the detection result. We trained our 2D and 3D CNNs using a dataset provided by Hamad Medical Corporation [31] composed of 165 transthoracic echocardiograms (TTE) belonging to anonymous patients.

The main contribution of this work is a fully automated pipeline for video segmentation and MI detection from echocardiography, whcih is also an indiscriminative pipeline that processes videos of different sizes, different frame rates and different resolutions. The proposed method is an end-to-end robust system that achieves 97.18% accuracy on data segmentation and 90.9% accuracy, 100% precision and 95% recall on MI detection. This system is robust in that it performs well with low quality videos corrupted with intense noise. It is also lightweight in that it does not require high memory or computational power in order to be executed, which makes the system adequate to be embedded in external devices.

In Section 2, we discuss existing research works related to our work. We then explain in Section 3 the pipeline architecture and discuss details related to the dataset. In Section 4, we explain the preprocessing techniques applied to the dataset which is used as input to a 2D CNN. In addition, we give details related to the 2D CNN architecture. We describe data preprocessing techniques applied to the processed videos before feeding it to the 3D CNN in Section 5, in addition to detailing the 3D CNN architecture. In Section 6, we describe the training processes and the evaluation metrics related to each model, followed by a discussion of the results. Finally, in Section 7, we give concluding remarks.

2 Related Work

Multiple image-processing based models that aim to evaluate the myocardial motion to detect cardiovascular deficiencies have been produced over the last few decades. In [32], a contour-based technique for detecting wall motion abnormality by analyzing the temporal pattern of normalized wall thickening was proposed. Epicardium and endocardium zones were manually extracted from 14 images representing real-life patients. Subsequently, AHA 17-segment model was used to detect regional wall changes in wall thickening with 88% of accuracy. In [33], existing quantitative approaches were applied and tested to identify regional LV abnormalities in patients with MI and wall motion abnormalities. A dataset of 4 different 2D echocardiography views and coronary angiography were used to calculate the deviations of the contractions of the regional segments of the LV wall. An abnormal segment was identified when its deviation value is inferior to the mean contraction estimated over 10 normal subjects. All the quantitative approaches that were evaluated achieved above 76% of accuracy.

The second approach of processing cardiovascular data mostly use ML and DL algorithms. In [34], 723,754 clinically acquired Echocardiographic tests representing 27,028 patients were acquired to predict 1-year mortality in patients who had encountered heart deficiencies. The data videos were divided into 12 groups such that each group represented a different cardiac view. Then, 12 3D CNN models were trained separately, such that each model was trained over one data group. The AUC values of the models ranged between 69% and 78%. The accuracy value of the 1-year mortality prediction in patients with heart abnormality records was 75%. [35] used DL in order to assess regional wall motion abnormality in Echocardiographic images. Data from 300 patients with history of MI were used and were divided into 3 groups such that each group of data represented a specific cardiac abnormality. Data from 100 healthy patients were also added to the data groups. Then, 10 versions of the same CNN architecture were trained and evaluated. The obtained CNN predictions were compared with the predictions made by expert cardiologists. The AUC curve produced by the cardiologists was similar to that produced by the CNNs (0.99 vs 0.98).

In [36], both electrocardiogram and serum analysis were used to detect AMI in patients who were suspected of having MI within one hour of their arrival to the care unit. The electrical activity of the heart produced by the 12-lead electrocardiogram were analyzed. Moreover, several chemical substances such as creatine kinase and myoglobin were measured. These parameters were combined to perform a logistic regression analysis that led to the detection of MI by 64% of accuracy, and 11% of false positive rate.

3 Methodology

One of the main goals of our work is to create a fully automated pipeline for LV segmentation and MI detection to assist technicians and cardiologists in the process of analyzing a patient's echocardiography. This system must be lightweight enough to be easily integrated into an embedded system, and as efficient and accurate as possible. In emergencies, for example, the data acquisition tend to be made quickly, which may impact the echocardiography video quality. Moreover, the majority of the echocardipgraphy machines used in hospitals produce low-quality videos of a frame rate below 30 frames per second (fps). In the following sections, we give an overview of the pipeline architecture and a description of the echocardiography videos acquired for this work.

3 .1 Pipeline Overview

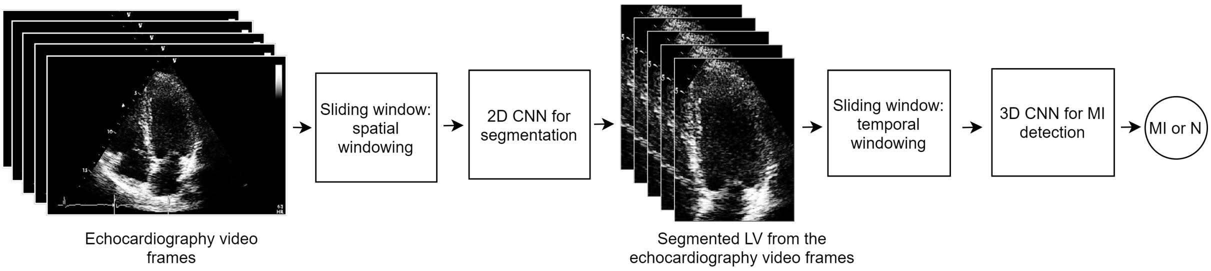
Echocardiography video frames
Sliding window: spatial windowing
2D CNN for segmentation
Segmented LV from the echocardiography video frames
Sliding window: temporal windowing
3D CNN for MI detection
MI or N

Fig. 1 Fully automated pipeline for MI detection, where the input is an echocardiography video and the output is the prediction results

Figure 1 illustrates the flow of the automated pipeline where the input consists of an echocardiography video called *echocardiography video frames*, and the output is the detection result. The video frames are processed by the sliding window technique which divides each frame into spatial windows of equal dimension. The spatial windows are passed through the 2D CNN to segment the LV from each frame's spatial windows. Once the segmented windows are produced, they are reassembled into segmented frames. These segmented frames are reassembled to produce a segmented video, where the order of appearance of each segmented frame is kept in the same order of appearance in the original echocardiography video. The segmented video frames are labelled in Figure 1 as *segmented LV from the echocardiography video frames.* These are then processed by another sliding window to produce temporal windows of the same dimensions. The temporal windows are then passed through a 3D CNN that classifies them into one of the following classes: abnormal (MI) or normal (N). The final class of the input video is estimated as the statistical mode of all the predictions of the frames constituting the video.

3 .2 Echocardiography Dataset

In collaboration with Hamad Medical Corporation in the State of Qatar, we were able to gather a dataset of 165 animated echocardiography videos, each from a distinct anonymous patient. The dataset was created by collecting various echocardiography tests from the hospital's archive. The patient's identities remain anonymous. The tests represent the A4C view, and have a frame rate of 25fps. The prevalent problem during data collection was the corruption of videos due to either noise or distorted representation of the A4C view, which usually consists in missing parts of the heart chambers that failed to be acquired during the echocardiography test. In this work, our dataset included both poor and good quality videos.

In accordance with the definition of MI abnormalities as stated in [4], this work focuses on learning the LV wall motion deformations in the A4C view. Figure 2 shows the A4C view as displayed in one video of our dataset. It contains four distinct heart chambers, numbered from 1 to 4, where 1 identifies the LV, 2 to 4 identifies the Right Ventricle, the Left Atrium and the Right Atrium, respectively.

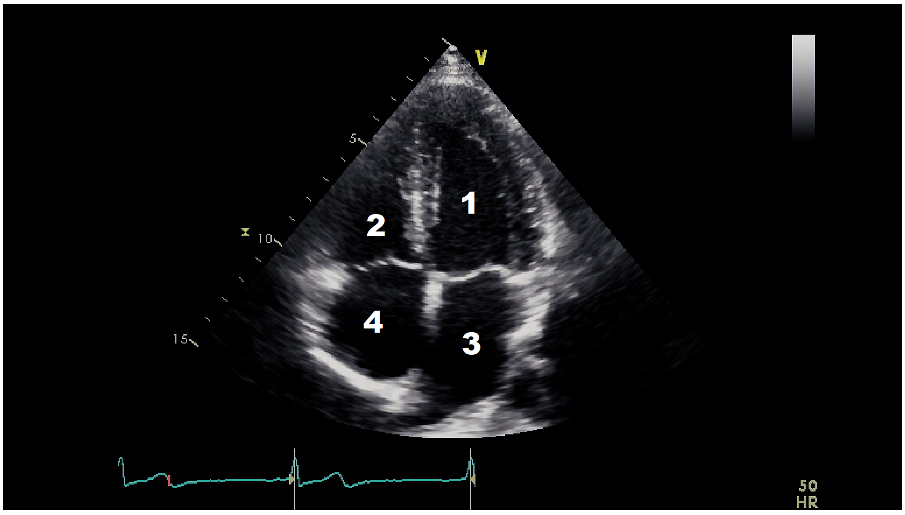

Fig. 2 Apical four-chamber view. The numbers from 1 to 4 marking the four different chambers correspond respectively to the LV, the right ventricle, the left atrium and the right atrium

Figure 3 represents captured frames representing the quality of several videos from our dataset, which varies from good to noisy. Figures from 3a to 3f correspond to distinct frames each captured from different videos. We notice that in Figure 3a the left wall of the LV is blurred. Also, in Figure 3b, the left wall of the LV is blurred and almost missing. In the same way, we observe that the totality of the LV wall is blurred in Figure 3c, and that the interior of the LV is disrupted with noise in Figure 3d. Finally, both Figure 3e and Figure 3f show acceptable LV representations, where the LV walls are captured and the chamber's interior is empty from noise. Moreover, since our study is centered on the LV chamber only, we purposely ignore the distortions of the rest of the cardiac chambers (Right Ventricle, Left Atrium and Right Atrium) in the dataset videos. For example, in Figure 3e, both the Left Atrium and the Right Atrium are partially cut from the view, however, this does not impact our study.

Hence, our final set of videos for segmentation consists of both clear and blurred video images of the LV chamber.

4 Video Segmentation with 2D CNN

The 2D CNN performs a supervised classification by learning to map the input echocardiography video to its adequate segmentation mask. Thus, we manually created segmentation masks that covers the LV chamber from the A4C view and discards the remaining chambers. The manually created segmentation masks were assigned to the dataset video frames as labels, and fed to the 2D CNN to learn the best segmentation mask from any given echocardiography video. The videos were normalized prior to training the 2D CNN by means of the sliding window technique due to differences in the dimensions of the frames.

4 .1 Data Preprocessing for 2D CNN

4 .1.1 Creating labels

The first step was preparing a labelled dataset, where each input is an echocardiography video frame, and each output is a corresponding segmentation mask. The segmentation masks were manually created and designed to cover the area of LV from the A4C in all the frames included in a given video. In each video, at least one cardiac cycle was performed, which means that we have at least one diastole (when the heart refills with blood) and one systole (when the heart pumps the blood) per video. The segmentation mask boundaries were determined such that they form a rectangle that encompasses the totality of the LV even on the frames where the heart is fully expanded, i.e. during diastole when the LV reaches its maximum volume. We assigned one segmentation mask per each echocardiography video. Consequently, the

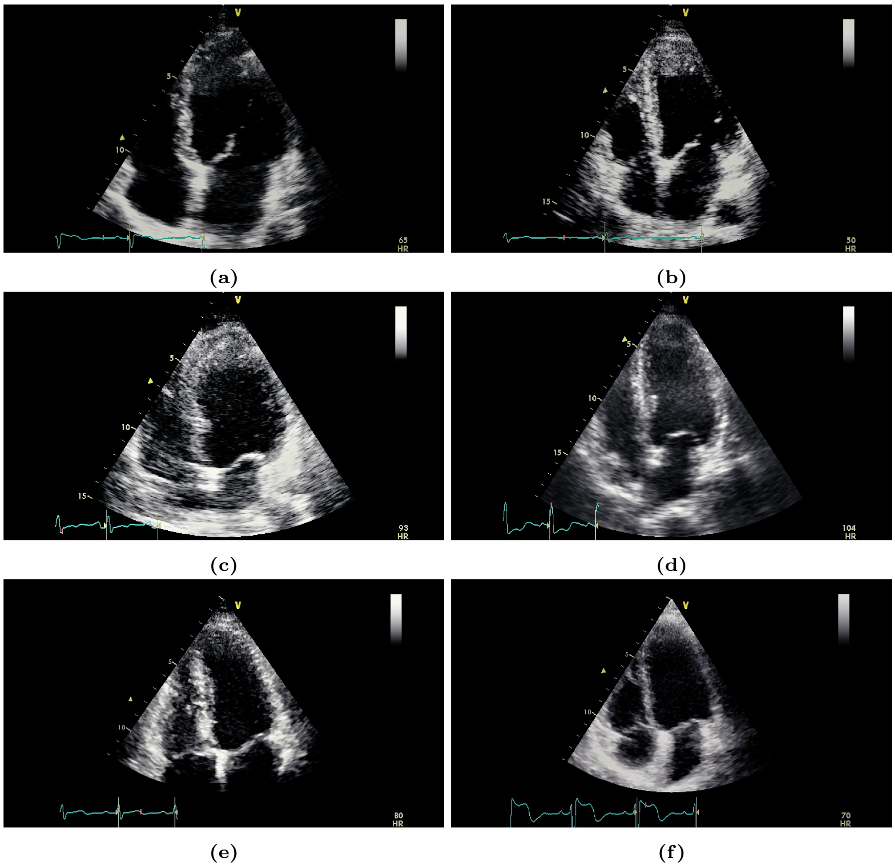

(a) **(b)**

(c) **(d)**

(e) **(f)**

Fig. 3 Captured frames from 6 different videos of our dataset, where each image from 3a to 3f corresponds to a distinct video. 3a Represents a blurred left wall in the LV, 3b represents a missing left wall in the LV, 3c represents blurred LV walls, 3d represents noise inside the LV, and 3e and 3f represent normal echocardiograms

segmentation mask assigned to a video was the same assigned to each of its frames. Thus, the final dataset that was used to train the 2D CNN contained the totality of the video frames as the input samples, and the totality of the segmentation masks as the labels or the output samples.

4 .1.2 Spatial windowing: segmentation process

The next step was to produce frames of the same spatial dimensions (frame size). Thereby, we opted for the sliding window technique to create spatial windows of fixed dimensions, and we applied the technique on both the input samples and the labels. The technique consists of extracting consecutive windows of equal dimensions with an overlap between two successive windows.

Normally, the dimension of the window must be less than or equal to the original dimension of the frame from which it was extracted. Also, the overlap should be less than the dimension of the window. In Figure 4, we illustrate the sliding window technique, where it extracts two successive windows with an overlap equal to 50%. The red square in the figure represents a window and the green square represents its successive window that overlaps with the read square by 50%.

By applying the sliding window technique on the dataset, we created windows of dimension equal to 150 × 150 pixels (px), with a 50% spatial overlap equal to 75 px. The dimensions of the windows are always less than the original dimensions of the video frames, where the smallest frame dimension in the input samples is equal to 422 × 636 px. In this manner, we uniformized and increased the input samples by producing a total of 108,127 windows.

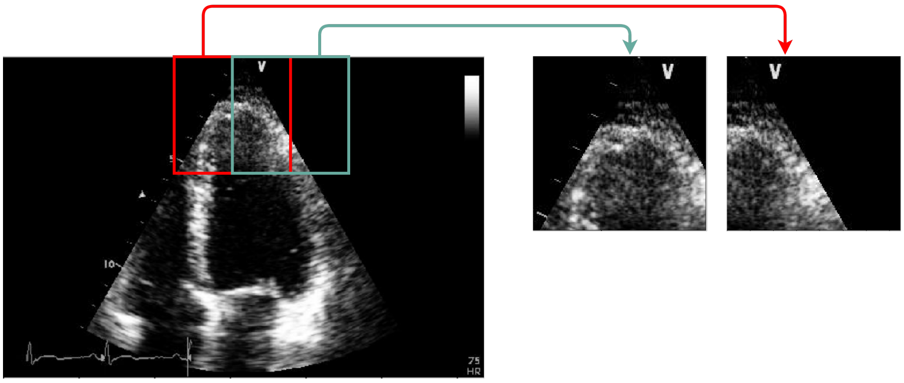

Fig. 4 Sliding window: the process of extracting two consecutive spatial windows from an frame with an overlap equal to 50% between the successive windows

The 2D CNN generates an estimation of a segmentation mask for an input window where each value within the segmentation mask is in the interval $[0, 1]$. We round these values to obtain a perfect mask with pixel values equal either 0 or 1. Once the segmentation mask corresponding to each window is estimated, the complete segmentation mask of a video frame is reconstructed using the inverse sliding window technique. The technique is performed by adding the successive estimated segmentation masks of every window from a certain frame with an overlap equal to 50% until we recover the entire frame. The reconstructed frame has the same dimension as the original frame cut from its video. With the same inverse sliding window technique, we recover all the segmentation video frames and also all the segmentation masks, where each mask corresponds to a frame. Then, having all the segmentation masks predicted for each frame of a given video, we aggregate these masks by means of statistical mode (i.e. the most represented value in each pixel is chosen) to form the segmentation mask corresponding to the totality of a video.

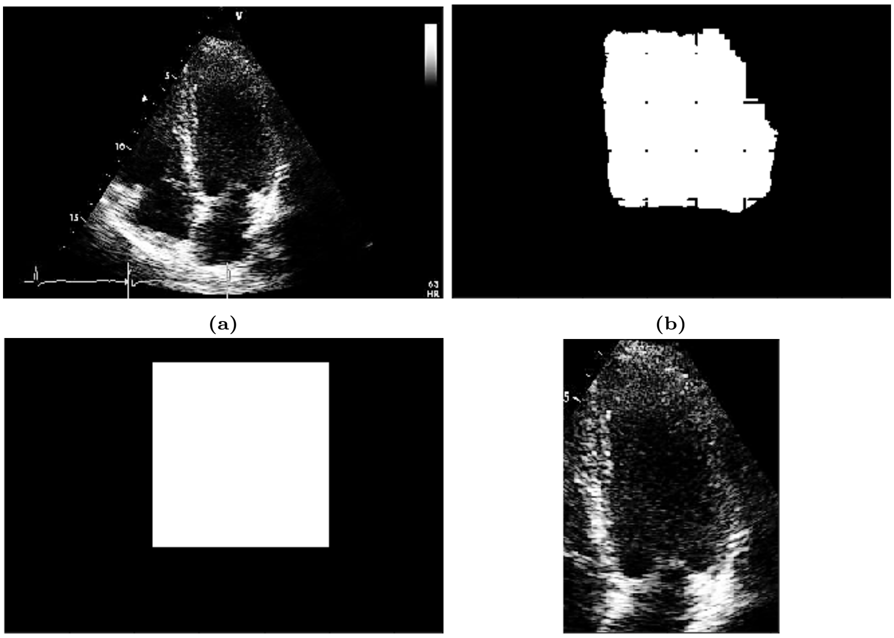

(a) (b)

(c) (d)

Fig. 5 Captured images from the different stages of the segmentation mask process applied to a video frame, where 5a represents the original video frame. 5b represents the segmentation mask corresponding to the frame (a) and obtained from the 2D CNN. 5c corresponds to the minimum bounding box of the predicted segmentation mask in 5b, and 5d is the segmented frame resulted from multiplying the original video frame 5a by the minimum bounding box in 5c

Figure 5 encapsulates the process of applying the predicted segmentation mask on a video frame. Figure 5a shows an original video frame, while Figure 5b shows its corresponding predicted mask recovered from the reverse sliding window technique, which appears as a set of points with undefined boundaries. Hence, to recover a rectangular-shaped segmentation mask we apply the minimum bounding box technique to enclose the estimated set of points into a rectangle and to produce a bounding box as shown in Figure 5c. Then, each video frame is multiplied by its corresponding bounding box to produce a segmented frame as shown in Figure 5d. The segmented frames belonging to the same video are then reassembled to produce a segmented video, where the order of appearance of each segmented frame is kept in its same order of appearance as in the original video. The segmented video has the same number of frames as the original video prior to any preprocessing, however, it has inferior frame sizes.

4 .2 2D CNN Architecture

Our 2D CNN architecture follows the encoder-decoder design common to CNNs developed for semantic segmentation problems [37]-[38]-[39]. Figure 6 illustrates the detailed configuration of the 2D CNN consisting of 3 convolutional layers with rectified linear unit (ReLU) as the activation function for each layer. Every convolutional layer is followed by a max pooling layer to reduce the dimension of the window. Then, the convolutional layers are followed by 3 transpose convolutional layers [40] with a stride equal to 2×2 in order to reacquire the initial input dimension. Each transpose layer uses a ReLU as its activation function. The last layer is a convolutional layer with a sigmoid activation function, which was selected to produce a predicted segmentation mask with pixel values equal to probabilities between the range of $[0, 1]$. The input and output dimensions are 150×150 px, which correspond to a segmentation mask adequate for the input window.

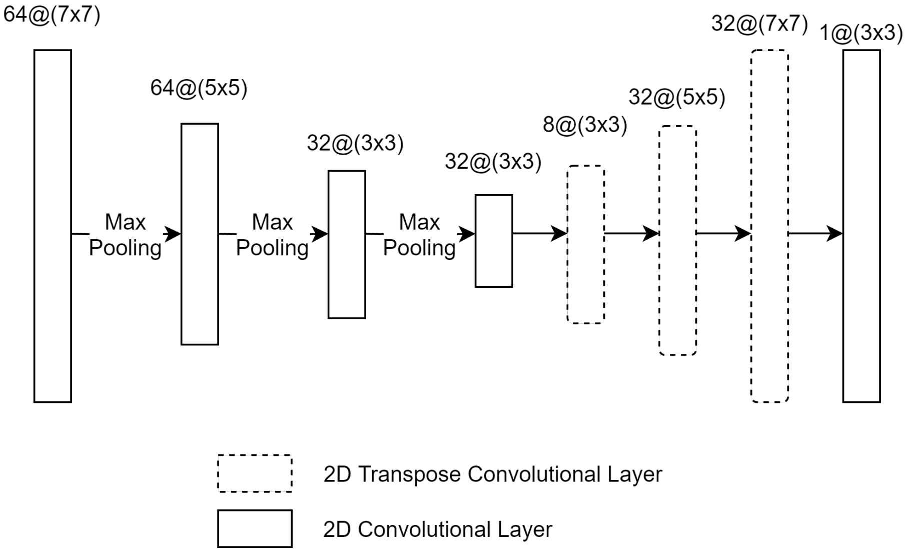

Fig. 6 The architecture of the 2D CNN

5 MI Detection with 3D CNN

In this section, we give details of MI detection with 3D CNN of segmented echocardiography videos obtained from a 2D CNN. However, these segmented videos have different number of frames and different dimensions. In the following section, we give preprocessing details of segmented videos.

5 .1 Data Preprocessing with 3D CNN

To solve the issue of differences in the spatial dimensions, all the video frames were scaled down to the smallest video size in the dataset. In our case, the smallest frame size from the segmented videos is equal to 236 × 183 px. Then, we applied the sliding window technique to the resized videos in order to obtain a uniform number of frames. The technique consists of extracting a temporal window created from a consecutive number of frames from a given video and repeating the process by going over all the video frames with respect to an overlap between two successive temporal windows. In general, the overlap size is inferior to the temporal window size. The technique allows dividing the dataset videos into smaller temporal windows of a fixed number of frames. It also allowed us to increase the number of samples for the 3D CNN from 165 segmented video to 2000 temporal windows. In our case, we applied the sliding window technique to extract temporal windows of size equal to 5, 7 and 9 frames per window, with an overlap equal respectively to 4, 6 and 8 frames (i.e. the sliding window moves forward by one window per step). By varying the size of the temporal windows, we created 3 different datasets that we used to train 3 different 3D CNN models.

We illustrate in Figure 7 the sliding window technique for a temporal window size equal to 5. The red window represents a temporal window consisting of 5 successive frames. The green window is the successive temporal window of the red one that also contains 5 frames, such that the first 4 frames from the green window are the same as the last 4 frames from the red window. The labels attributed to these temporal windows are the same as the labels of the video from which these windows were extracted.

Table 1 shows the number of the temporal windows obtained from the dataset videos by varying the frame number of the temporal windows. For a windows size equal to 5, 7 and 9, we obtained respectively 2841, 2511 and 2181 temporal windows from the dataset of the segmented videos.

Table 1 Number of windows obtained by applying the temporal sliding window technique with different window sizes

Size of the temporal window	Number of windows
5 frames	2841
7 frames	2511
9 frames	2181

In another experiment, we applied a sliding window technique that extracts spatio-temporal windows from the segmented videos in an attempt to avoid rescaling the videos to the smallest dimension. The technique consists of combining the temporal and spatial sliding window techniques at the same time. Even though this process resulted in a larger dataset, the predicted accuracies were lower than those obtained by simply resizing the segmented videos and

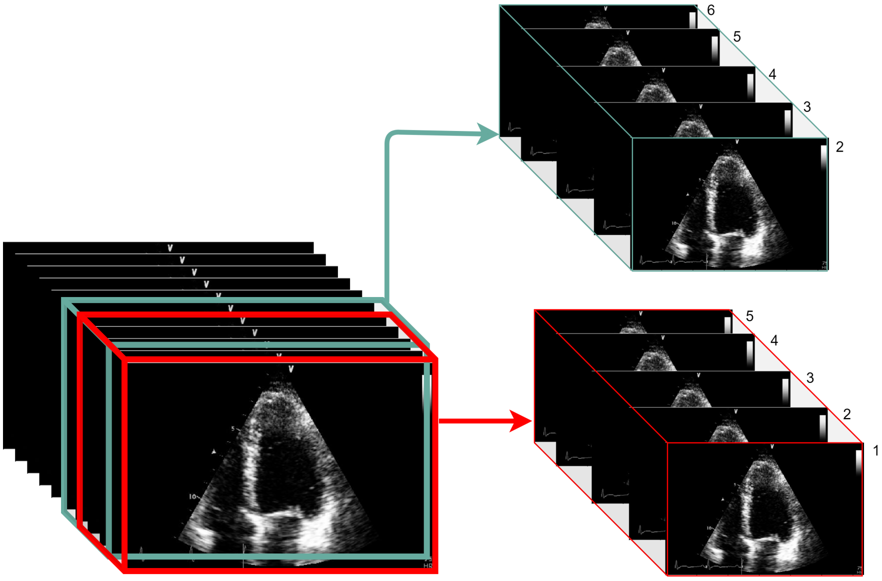

Fig. 7 Temporal sliding window depicting the process of extracting 2 consecutive temporal windows of size 5 frames, with an overlap equal to 4 frames between two consecutive windows

applying only temporal sliding window. Therefore, we concluded that the LV chamber should be fully preserved as a frame in the echocardiography video in order for the 3D CNN to capture the totality of its details throughout the process of learning. Cutting the LV chamber from a segmented video by a spatial sliding window will deteriorate the information and will result in a poorer model.

5 .2 3D CNN Architectures

In this section, we explain the architectures of the 3D CNN models used to train the 3 datasets separately. For each dataset, we used the same model architecture: same number of layers, same number of neurons and same activation functions. However, we changed the kernel size for each model to make it fit with the input dimension of the windows.

Figure 8 shows the architecture of the 3D CNN consisting of 4 3D convolutional layers, 4 2D max pooling layers, and 3 dense layers. The activation function used for all the layers, both convolutional and dense, except for the output layer, is ReLU. For the output layer, which consists of one neuron that contains the prediction probability, we used sigmoid activation function. Table 2 gives the details of the characteristics for each 3D CNN model.

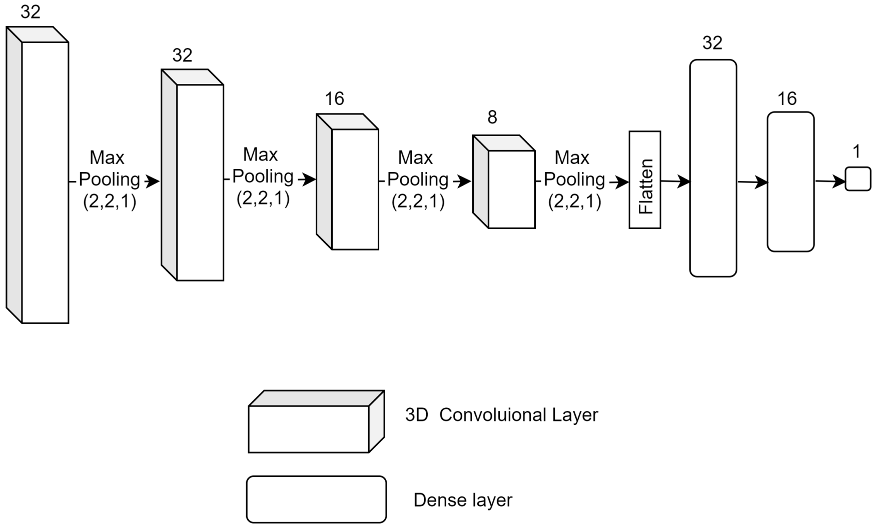

Fig. 8 The generic architecture of the 3D CNN used to train all the datasets

Table 2 3D CNN characteristics per layer according to the size of the temporal window

		Kernel size per window size		
Layer	No. of neurons	5	7	9
Conv3D	32	$(3,3,3)$	$(3,3,3)$	$(3,3,3)$
MaxPooling	-	$(2,2,1)$	$(2,2,1)$	$(2,2,1)$
Conv3D	32	$(3,3,2)$	$(3,3,3)$	$(3,3,3)$
MaxPooling	-	$(2,2,1)$	$(2,2,1)$	$(2,2,1)$
Conv3D	16	$(3,3,2)$	$(3,3,2)$	$(3,3,3)$
MaxPooling	-	$(2,2,1)$	$(2,2,1)$	$(2,2,1)$
Conv3D	8	$(3,3,1)$	$(3,3,2)$	$(3,3,3)$
MaxPooling	-	$(2,2,1)$	$(2,2,1)$	$(2,2,1)$
Flatten	-			
Dense	32			
Dense	16			
Dense	1			

6 Experiments and Results

6 .1 2D CNN: Training and Evaluation Metrics

In order to train the 2D CNN for the task of predicting segmentation masks, we normalized the data to values in the interval $[0, 1]$. Then, we divided the dataset into disjoint subsets for training and testing, consisting of 80% and 20% of the dataset, respectively. Next, we create a sub-set for the validation set, to fine-tune the hyper-parameters of the model, equal to 20% of the 80% of the training set. We trained the model for 100 epochs with a batch size equal to 256. The total trainable parameters of the 2D CNN are equal to 192,617. We used sigmoid activation function for the last layer, and RMSProp optimizer as the optimization function for the 2D CNN. To evaluate the model's performance we used the mean squared error (MSE) as the loss function. As a result, the MSE is defined as

$$MSE(w, \hat{w}) = \frac{1}{w_h w_w} \sum_{i=0}^{w_h-1} \sum_{j=0}^{w_w-1} [w_{(i,j)} - \hat{w}_{(i,j)}]^2. \tag{1}$$

In Eq. 1, w_h and w_w are the window's height and width, respectively, while w and $\hat{w}$ are the actual window and its corresponding prediction, respectively.

All relevant details regarding the training parameters of the 2D CNN are given in Table 3.

Table 3 2D CNN training parameters

Parameters	Values
Input samples (windows)	$86,502$ (80%)
Input shape	$(150,150)$
Output shape	$(150,150)$
Trainable parameters	$192,617$
Loss	MSE
Optimizer	RMSProp
Epochs	100
Batch size	256

6 .2 2D CNN: Results and Discussion

We evaluated the model using the test set by calculating the accuracy as

$$Accuracy(w, \hat{w}) = 1 - MSE(w, \hat{w}). \tag{2}$$

The model achieved 97.18% accuracy over the test set. While the accuracy is good, we believe that our results demonstrate that the segmentation masks predicted pixel-wise by the 2D CNN for the LV chamber from the A4C view are more precise than the manually extracted segmentations masks.

6 .3 3D CNNs: Training and Evaluation Metrics

For the 3D CNN experiments, we split the dataset into training and test sets consisting of 80% and 20% of the dataset, respectively. Since the MI detection is a binary classification, we ensured that the dataset is balanced with respect to N and MI classes. Then, we applied 5-fold cross-validation (CV) [41] on each 3D CNN model. We evaluated the trained models using their corresponding test sets. However, our goal is to predict the class of a complete echocardiography video rather than the class of a temporal window. Thus, to calculate the evaluation metrics of the 3D model over the task of MI detection per video, we assigned a prediction class to each video as the result of the statistical mode calculated over all the predicted classes of the windows constituting that video.

The evaluation metrics used to assess the performance of the models are

$$\begin{aligned} Precision &= \frac{True\ Positive}{True\ Positve + False\ Positive}, \\ Recall \quad &= \frac{True\ Positive}{True\ Positve + False\ Negative}, \ and \\ F1\ score \ &= 2\ \frac{Precision \times Recall}{precision + recall}. \end{aligned} \tag{3}$$

To train the models, we used the same loss function, learning rate, and optimizer, however, the input shape varies between the models as shown in Table 4. We used binary cross-entropy as the loss function, and the RMSProp optimizer with a learning rate equal to $1e^{-3}$. Per each fold, we trained the model for 100 epochs using a batch size equal to 8 samples. We calculated the evaluation metrics per video for each fold associated with each model.

To implement the 3D CNN models, we used the Python programming language and its open-source neural network library Keras [42]. We run the experiments on an NVIDIA Tesla P100 GPU server with 12GB of GPU memory.

Table 4 3D CNN models' training parameters per window size

	Window size		
Parameters	5	7	9
Input samples (windows)	2273	2009	1745
Input shape	(236,183,5)	(236,183,7)	(236,183,9)
Trainable parameters	57,977	68,345	74,105
Loss	Binary CrossEntropy		
Optimizer	RMSProp		
Learning rate	$1e^{-3}$		
Epochs per fold	100		
Batch size	8		

6 .4 3D CNNs: Results and Discussion

Table 5 shows the results of the evaluation metrics, as produced by the fully trained 3D models using 5-fold CV and calculated with their corresponding test sets. Only the highest, lowest and mean values are given.

The best results of our models were 90.9% of accuracy, 92.3% F1 score, 100% precision and 95% recall. However, the mean values for the evaluation metrics are slightly lower than the maximum values, and this is explained by the fact that the training sets contain distinct training samples, where some of the windows contain more noise and hence are of poorer quality than other windows. Therefore, even though all the sets contain balanced and equal proportions of samples representing both classification classes, some of the folds may contain more noisy samples than the remaining folds, which influences the learning performance of the model at each fold. Hence, the model trained over the dataset of windows with size equal to 5 frames, achieved 84.6% as the mean accuracy over the 5 folds of the CV, 86.1% as the mean value of the F1 score, 89% precision and 85.1% the mean value of the recall. Furthermore, we observe that the mean values of the evaluation metrics obtained from the dataset of windows equal to 7 frames, are slightly inferior to those attained from the dataset of windows with size equal to 5. Likewise, the mean values of the evaluation metrics achieved over the dataset of windows equal to 9 frames, are less than those obtained over the windows of size equal to 7 frames. The mean values of the metrics obtained from the second dataset (window size 7) are respectively equal to 82.5% of accuracy, 83.5% of F1 score, 83.5% of precision and 83.1% of recall, whereas, the values obtained from the third (window size 9) are respectively equal to 81.3% of accuracy, 83.1% of F1 score, 84.6% of precision and 82% of recall. Thus, we conclude that enlarging the size of the temporal window reduces the performance of the 3D CNN.

Table 5 3D CNN models' evaluation metrics per window size

		Window size		
Evaluation metrics		5	7	9
Accuracy	Max	90.3 %	**90.9 %**	90.0 %
	Mean	**84.6 %**	82.5 %	81.3 %
	Min	**77.1 %**	72.9 %	68.4 %
F1 score	Max	**92.3 %**	**92.3 %**	**92.3 %**
	Mean	**86.1 %**	83.5 %	83.1 %
	Min	**76.4 %**	75.0 %	68.4 %
Precision	Max	94.7 %	**100 %**	94.7 %
	Mean	**89.0 %**	83.5 %	84.6 %
	Min	73.0 %	**75.0 %**	72.2 %
Recall	Max	**95.0 %**	94.7 %	90.0 %
	Mean	**85.1 %**	83.1 %	82.0 %
	Min	65.0 %	**75.0 %**	65.0 %

7 Conclusion and Future Work

The main motivation of this work is to assist cardiologists with improving the MI detection accuracy by integrating DL and ML into the diagnostic process. This system replaces the time-consuming manual preprocessing by a fast and reliable LV segmentation, and improves MI detection by suggesting to doctors an alternative MI-prediction result of high accuracy within real-time. Our 2D CNN for video segmentation achieved a high accuracy of 97.18% in segmenting LV from the A4C, exceeding in time and precision manual preprocessing and showing that it could be very reliable and valuable to cardiologists. Moreover, our 3D CNN demonstrates that real-time prediction of MI from a patient's echocardiography is feasible and efficient. It achieved at best 90.9% accuracy, 100% precision, 92.3% F1 score and 95% recall. We believe that our 3D CNN assessment was impacted by the small number of video samples in our dataset. Noisy and low-quality echocardigraphy decreased the ability of the 3D CNN to extract features and detect MI from the segmented LV view. Nevertheless, our results demonstrates the robustness and efficiency of the models, which were able to detect MI in all the videos regardless of its quality. Accuracy, precision, recall as well as F1 score vary depending on the temporal window size. We relate this variability to the difference in the 3D CNN model's characteristics, which may alter the ability of the model to extract relevant prediction features with the given neuron and layer parameters. The 3D CNN models were built with the objective of assigning few layers and neurons that are able to extract relevant spatio-temporal features from the temporal windows without focusing on irrelevant details that would decreases the prediction accuracy. For our future work, we aim to merge our end-to-end automated pipeline into an embedded system using TensorRT [43]. In addition, we aspire to improve our model's results by enlarging the dataset with more echocardiography videos [44].

Acknowledgements

The authors wish to acknowledge the help of the State of Qatar and Hamad Medical Corporation for providing us with the medical data used in this work.

Declarations

Funding

The work of Sheela Ramanna and Christopher Henry was funded by the NSERC Discovery Grants Program (nos. 194376, 418413).

Conflicts of interest/Competing interests

There is no conflict of interest with the funders.

Consent to participate

All the Authors consent to the content of the manuscript.

References

1. Lawrence J. Laslett, Peter Alagona, Bernard A. Clark, Joseph P. Drozda, Frances Saldivar, Sean R. Wilson, Chris Poe, and Menolly Hart. The worldwide environment of cardiovascular disease: Prevalence, diagnosis, therapy, and policy issues. *Journal of the American College of Cardiology*, 60(25_Supplement):S1–S49, 2012.
2. World Health Organization cardiovascular diseases. `https://www.who.int/en/news-room/fact-sheets/detail/cardiovascular-diseases-(cvds)`. Accessed: 2020-09-14.
3. MD FESC Lüscher, Thomas F. Myocardial infarction: mechanisms, diagnosis, and complications. *European Heart Journal*, 36(16):947–949, 04 2015.
4. Kristian Thygesen, Joseph S. Alpert, Allan S. Jaffe, Bernard R. Chaitman, Jeroen J. Bax, David A. Morrow, and Harvey D. White. Fourth universal definition of myocardial infarction (2018). volume 72, pages 2231–2264. Journal of the American College of Cardiology, 2018.
5. Lei Lu, Min Liu, RongRong Sun, Yi Zheng, and Peiying Zhang. Myocardial infarction: Symptoms and treatments. *Cell Biochemistry and Biophysics*, 72, 07 2015.
6. Frans Van de Werf, Diego Ardissino, Dennis V Cokkinos, Keith A A Fox, Desmond Julian, and et. al. Management of acute myocardial infarction in patients presenting with st-segment elevation. the task force on the management of acute myocardial infarction of the european society of cardiology. *European heart journal*, 24:28–66, 01 2003.
7. Nestor Gahungu, Robert Trueick, Saiuj Bhat, Partho P. Sengupta, and Girish Dwivedi. Current challenges and recent updates in artificial intelligence and echocardiography. *Current Cardiovascular Imaging Reports*, 13(2), Feb 2020.
8. Thomas Davenport, Ravi Kalakota, and Dennis V Cokkinos. The potential for artificial intelligence in healthcare. *Future healthcare journal*, 6(2):94–98, 06 2019.
9. Girish Dwivedi, Kwan L. Chan, Matthias G. Friedrich, and Rob S.B. Beanlands. Cardiovascular imaging: New directions in an evolving landscape. *Canadian Journal of Cardiology*, 29(3):257 – 259, 2013.
10. Jeroen Bax and Victoria delgado. Advanced imaging in valvular heart disease. *Nature Reviews Cardiology*, 14, 01 2017.
11. Pamela S. Douglas, Manuel D. Cerqueira, Daniel S. Berman, Kavitha Chinnaiyan, Meryl S. Cohen, Justin B. Lundbye, Rajan A.G. Patel, Partho P. Sengupta, Prem Soman, Neil J. Weissman, Timothy C. Wong, Federico Asch, Timothy M. Bateman, Daniel S. Berman, Ginger Biesbrock, Jeffrey Brinker, David Brophy, Manuel Cerqueira, Kavitha Chinnaiyan, Meryl Cohen, Vasken Dilsizian, Pamela S. Douglas, Joel Dudley, Frederick Epstein, Linda Gillam, Justin Lundbye, Ben McCallister, Jagat Narula, Rajan A.G. Patel, David Reynolds, U. Joseph Schoepf, Partho P. Sengupta, Nishant Shah, Prem Soman, James E. Udelson, Uma S. Valeti, Mary Norine Walsh, R. Parker Ward, W. Guy Weigold, Neil J. Weissman, Richard D. White, David Wolinsky, Timothy C. Wong, and William A. Zoghbi. The future of cardiac imaging: Report of a think tank convened by the american college of cardiology. *JACC: Cardiovascular Imaging*, 9(10):1211 – 1223, 2016.
12. Chensi Cao, Feng Liu, Hai Tan, Deshou Song, Wenjie Shu, Weizhong Li, Yiming Zhou, Xiaochen Bo, and Zhi Xie. Deep learning and its applications in biomedicine. *Genomics, Proteomics & Bioinformatics*, 16, 03 2018.
13. Morgan P. McBee, Omer A. Awan, Andrew T. Colucci, Comeron W. Ghobadi, Nadja Kadom, Akash P. Kansagra, Srini Tridandapani, and William F. Auffermann. Deep learning in radiology. *Academic Radiology*, 25(11):1472 – 1480, 2018.
14. Rahul Kumar Sevakula, Wan-Tai M. Au-Yeung, Jagmeet P. Singh, E. Kevin Heist, Eric M. Isselbacher, and Antonis A. Armoundas. State&#x2010;of&#x2010;the&#x2010;art machine learning techniques aiming

to improve patient outcomes pertaining to the cardiovascular system. *Journal of the American Heart Association*, 9(4):e013924, 2020.

15. John S. Gottdiener, James Bednarz, Richard Devereux, Julius Gardin, Allan Klein, Warren J. Manning, Annitta Morehead, Dalane Kitzman, Jae Oh, Miguel Quinones, Nelson B. Schiller, James H. Stein, and Neil J. Weissman. American society of echocardiography recommendations for use of echocardiography in clinical trials: A report from the american society of echocardiography's guidelines and standards committee and the task force on echocardiography in clinical trials. *Journal of the American Society of Echocardiography", issn = "0894-7317*, 17(10):1086–1119, oct 2004.
16. R S Horowitz, J Morganroth, C Parrotto, C C Chen, J Soffer, and F J Pauletto. Immediate diagnosis of acute myocardial infarction by two-dimensional echocardiography. *Circulation*, 65(2):323–329, 1982.
17. Jonathan Gaudet, Jason Waechter, Kevin McLaughlin, André Ferland, Tomás Godinez, Colin Bands, Paul Boucher, and Jocelyn Lockyer. Focused critical care echocardiography. *Critical Care Medicine*, 44:1, 06 2016.
18. Joseph E. O'Boyle, Alfred F. Parisi, Markku Nieminen, Robert A. Kloner, and Shukri Khuri. Quantitative detection of regional left ventricular contraction abnormalities by 2-dimensional echocardiography: Comparison of myocardial thickening and thinning and endocardial motion in a canine model. *The American Journal of Cardiology*, 51(10):1732 – 1738, 1983.
19. Gill Wharton, Richard Steeds, Bushra Rana, Richard Wheeler, Smith N, David Oxborough, Brewerton H, Jane Allen, Chambers J, Julie Sandoval, Guy Lloyd, Prathap Kanagala, Matthew T, Massani N, and Richard Jones. A minimum dataset for a standard transthoracic echocardiogram, from the british society of echocardiography education committee. *Echo Research and Practice*, 2, 03 2015.
20. Mustafa Kurt, Kamran Shaikh, Leif Peterson, Karla Kurrelmeyer, Gopi Shah, Sherif Nagueh, Robert Fromm, Miguel Quinones, and William Zoghbi. Impact of contrast echocardiography on evaluation of ventricular function and clinical management in a large prospective cohort. *Journal of the American College of Cardiology*, 53:802–10, 03 2009.
21. Aleksandar N. Neskovic, Andreas Hagendorff, Patrizio Lancellotti, Fabio Guarracino, Albert Varga, Bernard Cosyns, Frank A. Flachskampf, Bogdan A. Popescu, Luna Gargani, Jose Luis Zamorano, Luigi P. Badano, and on behalf of the European Association of Cardiovascular Imaging. Emergency echocardiography: the European Association of Cardiovascular Imaging recommendations. *European Heart Journal - Cardiovascular Imaging*, 14(1):1–11, 01 2013.
22. Y. Nagata, Yuichiro Kado, Takeshi Onoue, K. Otani, Akemi Nakazono, Y. Otsuji, and M. Takeuchi. Impact of image quality on reliability of the measurements of left ventricular systolic function and global longitudinal strain in 2d echocardiography. *Echo Research and Practice*, 5:27 – 39, 2018.
23. Maleeha Qazi, Glenn Fung, Sriram Krishnan, Romer Rosales, Harald Steck, R. Bharat Rao, Don Poldermans, and Dhanalakshmi Chandrasekaran. Automated heart wall motion abnormality detection from ultrasound images using bayesian networks. page 519–525, 2007.
24. Chieh Chen Wu, Wen Ding Hsu, Md Mohaimenul Islam, Tahmina Nasrin Poly, Hsuan Chia Yang, Phung Anh (Alex) Nguyen, Yao Chin Wang, and Yu Chuan (Jack) Li. An artificial intelligence approach to early predict non-st-elevation myocardial infarction patients with chest pain. *Computer Methods and Programs in Biomedicine*, 173:109–117, may 2019.
25. Yudong Zhu, Maria Drangova, and Norbert J. Pelc. Fourier tracking of myocardial motion using cine-pc data. *Magnetic Resonance in Medicine*, 35(4):471–480, 1996.
26. Abhishek Mishra, Pranab Dutta, and M.K. Ghosh. A ga based approach for boundary detection of left ventricle with echocardiographic image sequences. *Image and Vision Computing*, 21:967–976, 10 2003.
27. Mingqiang Chen, Lin Fang, Qi Zhuang, and Huafeng Liu. Deep learning assessment of myocardial infarction from mr image sequences. *IEEE Access*, PP:1–1, 01 2019.
28. Sukrit Narula, Khader Shameer, Alaa Mabrouk Salem Omar, Joel T. Dudley, and Partho P. Sengupta. Machine-learning algorithms to automate morphological and func-

tional assessments in 2d echocardiography. *Journal of the American College of Cardiology*, 68(21):2287–2295, 2016.

29. K. E. T. Upendra, G. A. C. Ranaweera, N. H. A. P. Samaradiwakara, A. Munasinghe, K. L. Jayaratne, and M. I. E. Wickramasinghe. Artificial neural network application in classifying the left ventricular function of the human heart using echocardiography. In *2018 National Information Technology Conference (NITC)*, pages 1–6, 2018.
30. Ioanna Kosmidou, Björn Redfors, Harry P. Selker, Holger Thiele, Manesh R. Patel, James E. Udelson, E. Magnus Ohman, Ingo Eitel, Christopher B. Granger, Akiko Maehara, Ajay Kirtane, Philippe Généreux, Paul L. Jenkins, Ori Ben-Yehuda, Gary S. Mintz, and Gregg W. Stone. Infarct size, left ventricular function, and prognosis in women compared to men after primary percutaneous coronary intervention in st-segment elevation myocardial infarction: results from an individual patient-level pooled analysis of 10 randomized trials. *European Heart Journal*, 38(21):1656–1663, 04 2017.
31. Hamad medical corporation. `https://www.hamad.qa/EN/Pages/default.aspx`. Accessed: 2020-09-24.
32. Mai Wael, El-Sayed Ibrahim, and Ahmed S. Fahmy. Detection of lv function abnormality using temporal patterns of normalized wall thickness. *Journal of Cardiovascular Magnetic Resonance*, 17:47, 02 2015.
33. P F Moynihan, A F Parisi, and C L Feldman. Quantitative detection of regional left ventricular contraction abnormalities by two-dimensional echocardiography. i. analysis of methods. *Circulation*, 63(4):752–760, 1981.
34. Alvaro Ulloa, Linyuan Jing, Christopher W. Good, David P. vanMaanen, Sushravya Raghunath, Jonathan D. Suever, Christopher D. Nevius, Gregory J. Wehner, Dustin N. Hartzel, Joseph B. Leader, Amro Alsaid, Aalpen A. Patel, H. Lester Kirchner, Christopher M. Haggerty, and Brandon K. Fornwalt. A deep neural network predicts survival after heart imaging better than cardiologists. *CoRR*, abs/1811.10553, 2018.
35. Kenya Kusunose, Takashi Abe, Akihiro Haga, Daiju Fukuda, Hirotsugu Yamada, Masafumi Harada, and Masataka Sata. A deep learning approach for assessment of regional wall motion abnormality from echocardiographic images. *JACC: Cardiovascular Imaging*, 13, 05 2019.
36. E. M. Ohman, C. Casey, J. R. Bengtson, D. Pryor, W. Tormey, and J. H. Horgan. Early detection of acute myocardial infarction: additional diagnostic information from serum concentrations of myoglobin in patients without st elevation. *British heart journal*, 163(6):335–338, 05 1990.
37. V. Badrinarayanan, A. Kendall, and R. Cipolla. Segnet: A deep convolutional encoder-decoder architecture for image segmentation. *IEEE Transactions on Pattern Analysis and Machine Intelligence*, 39(12):2481–2495, 2017.
38. Yongfeng Xing, Luo Zhong, and Xian Zhong. An encoder-decoder network based fcn architecture for semantic segmentation. *Wireless Communications and Mobile Computing*, 2020:1–9, 07 2020.
39. Victor Alhassan, Christopher J. Henry, Sheela Ramanna, and Christopher Storie. A deep learning framework for land-use/land-cover mapping and analysis using multispectral satellite imagery. *Neural Computing and Applications*, 32, 06 2020.
40. Vincent Dumoulin and Francesco Visin. A guide to convolution arithmetic for deep learning. pages 18–23, 03 2016.
41. Payam Refaeilzadeh, Lei Tang, and Huan Liu. Cross-validation. pages 532–538, 2009.
42. François Chollet et al. Keras. `https://keras.io`, 2015.
43. TensorRT cardiovascular diseases. `https://developer.nvidia.com/tensorrt-getting-started`. Accessed: 2021-02-16.
44. Ali Madani, Jia Ong, Anshul Tibrewal, and Mohammad Mofrad. Deep echocardiography: data-efficient supervised and semi-supervised deep learning towards automated diagnosis of cardiac disease. *npj Digital Medicine*, 1, 12 2018.